OPEN ACCESS

University of BRISTOL

Guckenheimer, J., & Osinga, H. M. (2011). The singular limit of a Hopf bifurcation.

Early version, also known as pre-print

Link to publication record in Explore Bristol Research
PDF-document

University of Bristol - Explore Bristol Research

General rights

The singular limit of a Hopf bifurcation

John Guckenheimer

Mathematics Department, Cornell University, Ithaca, NY 14853, USA

Hinke M. Osinga

Bristol Centre for Applied Nonlinear Mathematics, Department of
Engineering Mathematics,
University of Bristol, Bristol BS8 1TR, United Kingdom

Abstract

Hopf bifurcation in systems with multiple time scales takes several forms, depending upon whether the bifurcation occurs in fast directions, slow directions or a mixture of these two. Hopf bifurcation in fast directions is influenced by the singular limit of the fast time scale, that is, when the ratio ε of the slowest and fastest time scales goes to zero. The bifurcations of the full slow-fast system persist in the fast subsystem obtained from this singular limit. However, the Hopf bifurcation of the fast subsystem does not necessarily have the same criticality as the corresponding Hopf bifurcation of the full slow-fast system, even in the limit $\varepsilon \to 0$ when the two bifurcations occur at the same point. We investigate this situation by presenting a simple slow-fast system that is amenable to a complete analysis of its bifurcation diagram. In this model, the family of periodic orbits that emanates from the Hopf bifurcation accumulates onto the corresponding family of the fast subsystem in the limit as $\varepsilon \to 0$; furthermore, the stability of the orbits is dictated by that of the fast subsystem. We prove that a torus bifurcation occurs $O(\varepsilon)$ near the Hopf bifurcation of the full system when the criticality of the two Hopf bifurcations is different.

1   Introduction

Dynamical systems with multiple time scales are common models for natural phenomena such as chemical reactions, electrical circuits, lasers, and biological processes; see [2] and references therein. These systems exhibit dynamical behaviors that result from interactions of the different time scales. Numerical methods for simulating single-time-scale models fail to capture some of these

dynamics, so it is often easier to begin with an analysis of singular limits in which the ratio of time scales becomes infinite. Along with much of the current research in this area, this paper investigates slow-fast systems of the form

$$\begin{cases} \varepsilon \dot{x} &= f(x, y), \\ \dot{y} &= g(x, y), \end{cases} \tag{1}$$

where the small parameter ε explicitly represents the ratio between two time scales and the time variable is on the slow time scale.

The singular limit $\varepsilon = 0$ of system (1) is a *differential-algebraic* system. Trajectories are confined to the *critical manifold* $f = 0$. Existence of solutions to this DAE may fail at *fold* points where the critical manifold has a tangent in the subspace of fast variables. Rescaling time to the fast time scale in system (1) produces

$$\begin{cases} \dot{x} &= f(x, y), \\ \dot{y} &= \varepsilon \, g(x, y), \end{cases} \tag{2}$$

for which the singular limit $\varepsilon = 0$ is the *layer equation*. The variable y acts as a parameter in the layer equation, which is also called the *fast subsystem* or *frozen system*. The flow of system (1) approaches that of the layer equations off the critical manifold. Thus, analysis of the singular limit of system (1) utilizes both the DAE and the layer equations: stable equilibria of the layer equations approximate *attracting slow manifolds* along which motion has a singular limit described by the DAE.

The earliest example of periodic slow-fast dynamics is the relaxation oscillation, introduced by Van der Pol [15, 16]: a periodic orbit consists of segments that alternately flow along attracting slow manifolds to a fold where they then *jump* along a trajectory of the layer equations to another attracting slow manifold. Periodic orbits or more complicated attractors of the layer equations of system (2) with $\varepsilon = 0$ may give rise to more complicated dynamical behaviors like bursting and mixed-mode oscillations of the "full" system with $\varepsilon > 0$. Bifurcations within the layer equations locate possible transitions in which trajectories transition from one type of attractor to another as the slow variables evolve. The analysis of these bifurcations, thus, serves as a starting point for investigations of the dynamics of the full system. This paper describes a curious phenomenon in which bifurcation analysis of the layer equations gives information about the full system that initially appears to be misleading.

Equilibria of the slow-fast system (1) always occur on its critical manifold. Away from folds, the Jacobian at an equilibrium has invariant subspaces that lie close to the layer $y = $ constant with eigenvalues of large magnitudes $O(\varepsilon^{-1})$ and close to the tangent space of the critical manifold with eigenvalues of magnitudes $O(1)$. In a family of systems, Hopf bifurcations may occur with a center manifold in either of these subspaces. Eigenvalues of intermediate magnitudes arise when the center manifold involves both slow and fast directions; this case is called *singular* Hopf bifurcation, and it only occurs near folds of slow-fast systems [1]. The focus of this paper is Hopf bifurcation where the center subspace lies close to a layer $y = $ constant. Note that this requires that the fast variable x of the system has dimension at least two. We give a careful study of the singular limit of these Hopf bifurcations as $\varepsilon \to 0$.

In addition to Hopf bifurcation of the full system (1) or (2), the layer equations (2) with $\varepsilon = 0$ can undergo *dynamic* Hopf bifurcation on its critical manifold as y varies. These Hopf bifurcations will be associated with a Hopf bifurcation of the full system only if $g = 0$ at the bifurcation point; otherwise the full system does not have an equilibrium near the dynamic Hopf bifurcation. Instead, there is a slow manifold in which trajectories flow on the slow time scale while their transverse stability in the fast directions changes. Due to the splitting of the Jacobian of the full system, Hopf bifurcations of the full system with $O(\varepsilon^{-1})$ eigenvalues always give rise to Hopf bifurcations of the layer equations in the singular limit.

Hopf bifurcations have normal forms: on center manifolds these take the form

$$\begin{cases} \dot{r} &= r\,(\lambda + a\,r^2) + o(r^3), \\ \dot{\vartheta} &= \omega + b\,r^2 + o(r^2), \end{cases} \tag{3}$$

when written in cylindrical coordinates (r, ϑ) with parameter λ. The coefficient a is the *first Lyapunov coefficient* whose magnitude scales with r^2. The bifurcation is subcritical and unstable periodic orbits emerge from the equilibrium when $a > 0$, while the bifurcation is supercritical and stable periodic orbits emerge from the equilibrium when $a < 0$; see [4] for more details. The curious phenomenon studied here is that the sign of the first Lyapunov coefficient can change discontinuously at the singular limit of system (2). This behavior has been observed, for example, in [18, 19] and was studied in more detail by Zhang *et al.* in the context of model-reduction techniques that are common in physiological applications [11]. There are precursors to

3

this phenomenon that appear in center manifold reduction: the formula for the first Lyapunov coefficient includes terms from variables transverse to the center manifold [12]. We complement these studies by drawing a connection between the discrepancy in signs of the first Lyapunov coefficient and a torus bifurcation: our main result is the following theorem.

Theorem 1.1. *Assume that the slow-fast system* (2) *undergoes a Hopf bifurcation* H *with center subspace lying close to a layer* $y = $ constant. *Let* $\ell_1(\varepsilon)$ *be the first Lyapunov coefficient of* H *and define* $\ell_1(0) = \lim_{\varepsilon \to 0} \ell_1(\varepsilon)$. *Now consider the limit of* H *as* $\varepsilon \to 0$ *as a Hopf bifurcation of the layer equations of system* (2), *which we denote* $\mathsf{H}_{\mathrm{crit}}$, *and let* $\ell_1(\mathrm{layer})$ *be the corresponding first Lyapunov coefficient in these layer equations. Then, if the signs of* $\ell_1(0)$ *and* $\ell_1(\mathrm{layer})$ *are different, system* (2) *has a torus bifurcation that occurs for parameters* $O(\varepsilon)$ *away from* H.

This paper is organized as follows. In the next section we investigate the singular limit of Hopf bifurcations in the well-known Hindmarsh–Rose model. This is followed by a simpler slow-fast system for which we give a complete analysis of the singular limit of its Hopf bifurcations: in Section 3 we discuss the relationship between Hopf bifurcation of system (2) and its singular limit in the context of this model. The connection with a torus bifurcation is explained in Section 3.3, where we also show that the invariant tori in this model are neutrally stable, unlike those in a generic slow-fast family undergoing Hopf bifurcation in its fast variables. The proof of Theorem 1.1 is discussed in Section 3.4. We end with conclusions in Section 4.

2 Motivating example

Neurons are typically modeled using Hodgkin–Huxley formalism and include equations for the membrane potential, gating variables of ionic currents, and sometimes an additional equation for calcium concentration that does not feature in the original Hodgkin–Huxley equations [7]. Hindmarsh and Rose [6] introduced simplified polynomial equations that exhibit the same types of bursting dynamics seen in models that follow the Hodgkin–Huxley formalism; see [13] in this issue. Here, we investigate the Hindmarsh–Rose-type

model from [14, 20] that is given by

$$
\begin{cases}
\dot{x} &= s\,a\,x^3 - s\,x^2 - y - b\,z, \\
\dot{y} &= (x^2 - y), \\
\dot{z} &= \varepsilon\,(s\,a_1\,x + b_1 - k\,z).
\end{cases}
\tag{4}
$$

We use $a = 0.5$, $b = 1$, $a_1 = -0.1$ and $k = 0.2$ throughout and study how the time-scale separation ε influences a Hopf bifurcation H that arises when varying the parameter b_1 for two different choices of s, namely, $s = -1.61$ and $s = -2.6$. The singular limit $\varepsilon = 0$ provides information about the dynamics of system (4) for small enough $\varepsilon > 0$. Indeed, the bursting patterns of neurons are effectively classified in terms of the bifurcation diagram generated from the fast subsystem; see [8, 17] and also [13] in this issue.

The layer equations of (4) are defined on the (x, y)-plane, where z acts as a parameter. The layer equations have a z-dependent S-shaped curve of equilibria that forms the critical manifold S_{crit}. One of the two fold points of S_{crit} gives rise to a bistable regime that ends in a Hopf bifurcation, which we denote $\mathsf{H}_{\mathrm{crit}}$. A family Γ_{crit} of periodic orbits emanates from $\mathsf{H}_{\mathrm{crit}}$. The two cases $s = -1.61$ and $s = -2.6$ are representative for the situations where $\mathsf{H}_{\mathrm{crit}}$ is supercritical, so Γ_{crit} is attracting, and $\mathsf{H}_{\mathrm{crit}}$ is subcritical, so Γ_{crit} is repelling, respectively. We want to investigate how $\mathsf{H}_{\mathrm{crit}}$ influences the behaviour of (4) as ε becomes positive and b_1 is varied. Note that b_1 only appears in the z-equation of (4), which means that S_{crit} and Γ_{crit} do not depend on b_1. Hence, in the limit as $\varepsilon \to 0$, the Hopf bifurcation H of the full system is equal to $\mathsf{H}_{\mathrm{crit}}$.

For each choice of s, an (ε, b_1)-dependent curve of Hopf bifurcations emanates from the fold point that starts the bistable regime in the singular limit. This fold point for $\varepsilon = 0$ lies at the origin of (x, y, z, b_1)-space, independent of s, and it is the limit of singular Hopf bifurcation points [1] that occur when $\varepsilon > 0$ is small. Figure 1(a) shows the locus of Hopf bifurcations in the (ε, b_1)-plane for the two choices of s; the corresponding Lyapunov coefficients ℓ_1 are shown in Figure 1(b). The two cases appear to be rather similar: the curve of Hopf bifurcations is subcritical as it emanates from the origin in the (ε, b_1)-plane; note that the positive segment of the curve in the (ε, ℓ_1)-plane in Figure 1(b) is not shown in its entirety up to $\varepsilon = 0$. Soon after the singular Hopf bifurcation, as b_1 decreases and ε increases, the curve passes through a degenerate Hopf bifurcation point and the criticality changes to supercritical, that is, $\ell_1 < 0$. We are interested in what happens in the singular limit as ε starts to decrease again and the curve of Hopf bifurcations reaches $\varepsilon = 0$ at a
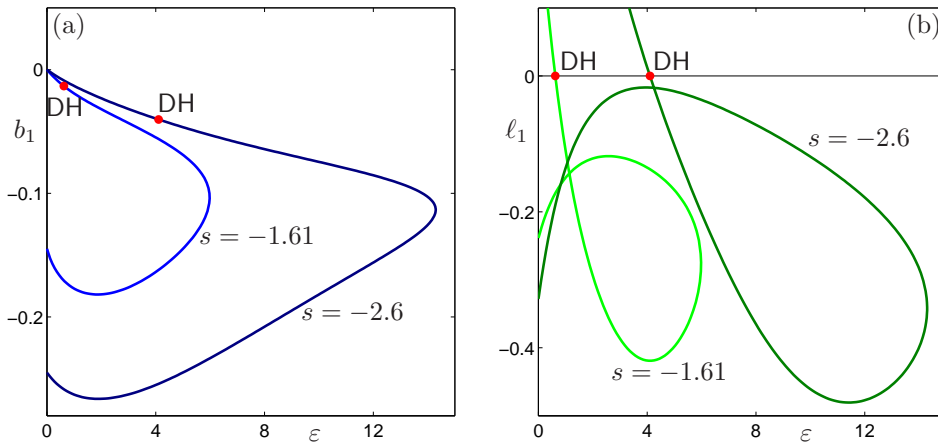
5

Figure 1: Loci of Hopf bifurcation for $s = -1.61$ and $s = -2.6$ in the (ε, b_1)-plane are shown in panel (a), along with the corresponding Lyapunov coefficients ℓ_1 versus ε in panel (b). For both cases the curve of Hopf bifurcations is subcritical as it emanates from the origin in the (ε, b_1)-plane; as b_1 decreases the curve passes through a degenerate Hopf bifurcation point and becomes supercritical, that is, $\ell_1 < 0$.

value $b_1 \ll 0$ that corresponds to the point where the equilibrium lies exactly at $\mathsf{H}_{\mathrm{crit}}$ on S_{crit}, which is at $b_1 \approx -0.1449$ for $s = -1.61$ and $b_1 \approx -0.2450$ for $s = -2.6$.

Let us first consider the case $s = -1.61$ where $\mathsf{H}_{\mathrm{crit}}$ is also supercritical. Figure 2 illustrates the Hopf bifurcation of (4) as b_1 is varied for $\varepsilon = 0.1$ in row (a) and $\varepsilon = 0.01$ in row (b). The first column shows the bifurcation diagram projected onto the (b_1, x)-plane, where both maxima and minima are shown of the family $\Gamma(b_1)$ of periodic orbits that emanates from the Hopf bifurcation point. Both Figures 2(a1) and (b1) show the classical bifurcation diagram of a stable equilibrium losing stability in a supercritical Hopf bifurcation, denoted H; this bifurcation H occurs at $b_1 \approx -0.1518$ when $\varepsilon = 0.1$ and at $b_1 \approx -0.1457$ when $\varepsilon = 0.01$. The second column of Figure 2 shows the familiy of equilibria and $\Gamma(b_1)$ projected onto (x, y, z)-space along with the critical manifolds S_{crit} and Γ_{crit}. For both choices of ε, the effect of varying b_1 is that the equilibrium of (4) moves along S_{crit} and through $\mathsf{H}_{\mathrm{crit}}$; it lies at $\mathsf{H}_{\mathrm{crit}}$ when $b_1 \approx -0.1449$. Hence, as b_1 increases, the actual Hopf bifurcation H of (4) occurs slightly before the equilibrium reaches $\mathsf{H}_{\mathrm{crit}}$, and
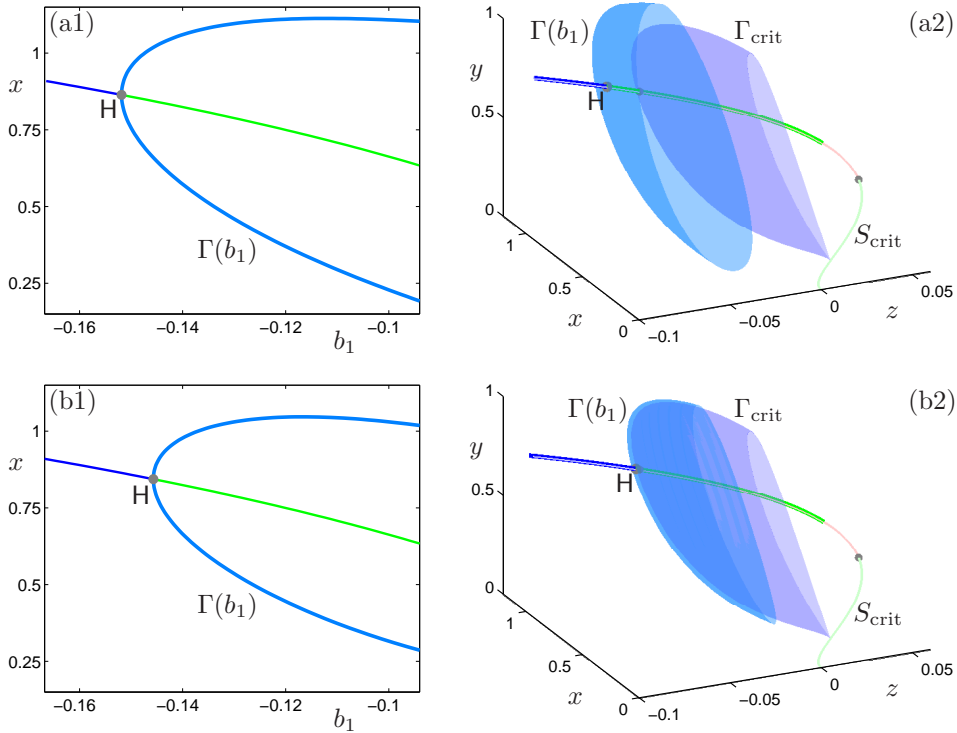
6

Figure 2: System (4) with $s = -1.61$ and $\varepsilon > 0$ small enough undergoes a supercritical Hopf bifurcation as b_1 varies; the case $\varepsilon = 0.1$ is shown in row (a) and $\varepsilon = 0.01$ in row (b). The first column shows the bifurcation diagram, where we plot x versus b_1; both maxima and minima in x of the emanating family $\Gamma(b_1)$ of periodic orbits are shown. The second column shows these b_1-dependent families of equilibria and periodic orbits in (x, y, z)-space, where z is plotted along a horizontal axis; overlayed are the critical manifold S_{crit} and the family Γ_{crit} of periodic orbits of the fast subsystem.

Figures 2(a2) and (b2) illustrate how the distance to H_{crit} decreases with ε. In fact, not only the Hopf bifurcation itself converges to H_{crit}, but also the family $\Gamma(b_1)$ accumulates onto Γ_{crit} as $\varepsilon \to 0$.

Let us now consider the case $s = -2.6$ where H is supercritical for $\varepsilon > 0$ small enough, while H_{crit} is subcritical. Figure 3 shows the situation for $s = -2.6$ in the same way as was done for $s = -1.61$ in Figure 2. Fig-
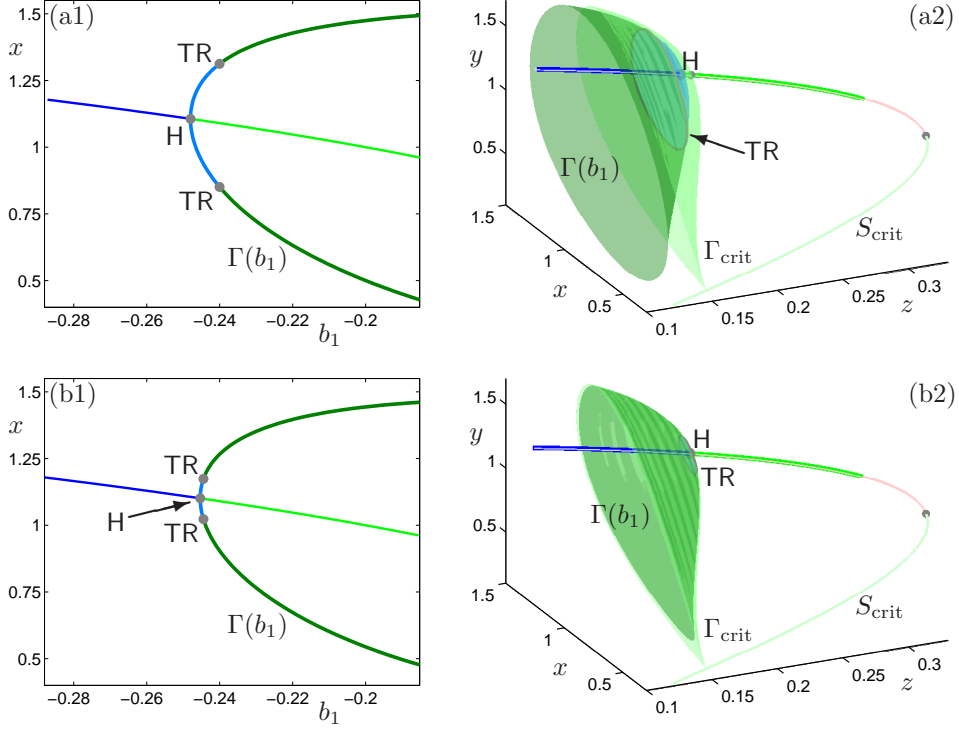
Figure 3: System (4) with $s = -2.6$ and $\varepsilon > 0$ small enough undergoes a supercritical Hopf bifurcation as b_1 varies, which is quickly followed by a torus bifurcation that renders the emanating family of periodic orbits unstable; the case $\varepsilon = 0.1$ is shown in row (a) and $\varepsilon = 0.01$ in row (b). The first column shows the bifurcation diagram, where we plot x versus b_1; both maxima and minima in x of the emanating family $\Gamma(b_1)$ of periodic orbits are shown. The second column shows these b_1-dependent families of equilibria and periodic orbits in (x, y, z)-space, where z is plotted along a horizontal axis; overlaid are the critical manifold S_{crit} and the family Γ_{crit} of periodic orbits of the fast subsystem, which has a subcritical rather than a supercritical Hopf bifurcation.

ures 3(a1) and (b1) show the classical bifurcation diagram of a stable equilibrium losing stability in a supercritical Hopf bifurcation, though now $\Gamma(b_1)$

8

becomes unstable soon after the Hopf bifurcation when a torus bifurcation, labeled TR, occurs; to be precise, H and TR occur at $b_1 \approx -0.2480$ and $b_1 \approx -0.2405$ for $\varepsilon = 0.1$, and at $b_1 \approx -0.2453$ and $b_1 \approx -0.2446$ for $\varepsilon = 0.01$, respectively. Hence, TR lies closer to H for $\varepsilon = 0.01$, in panel (b1), than for $\varepsilon = 0.1$, in panel (a1). The second column of Figure 3 illustrates that H occurs slightly before but increasingly closer to the point where the equilibrium on S_{crit} reaches H_{crit}, which is when $b_1 \approx -0.2450$. Furthermore, just as in Figure 2 the projection of $\Gamma(b_1)$ onto (x, y, z)-space accumulates onto Γ_{crit}, despite the fact that Γ_{crit} is a family that emanates from a subcritical rather than a supercritical Hopf bifurcation.

Figures 2 and 3 illustrate that H_{crit} and Γ_{crit} appear to be the limits of H and $\Gamma(b_1)$ as $\varepsilon \to 0$, even if the criticality of H_{crit} does not match the criticality of H. In fact, the Lyapunov coefficient ℓ_{crit} associated with H_{crit} is typically not equal to the limit as $\varepsilon \to 0$ of the Lyapunov coefficient ℓ_1 associated with H. Due to the special form of (4), It is not hard to use [9] and derive ℓ_{crit} explicitly as

$$\ell_{\mathrm{crit}} = \ell_{\mathrm{crit}}(s) = \frac{3\,s^2\,(7 + 4\,s)}{s - 2\,\sqrt{4\,s^2 + 6\,s}}. \tag{5}$$

We compute ℓ_1 in Figure 1(b) with MATCONT [3], but scaled the computed values by $\frac{1}{2}$. The reason for this is that the implementation in MATCONT [3] is based on the derivation by Kuznetsov in [12]; due to the difference in normalization of the eigenvectors, the value computed by MATCONT [3] is twice that of the coefficient obtained using the derivation by Guckenheimer and Holmes in [4], which is also used in [9]. We used the convention from [4] throughout this paper. Equation (5) leads to $\ell_{\mathrm{crit}} \approx -1.3223$ for $s = -1.61$ and $\ell_{\mathrm{crit}} \approx 7.3630$ for $s = -2.6$, but as can be observed from Figure 1(b), we have $\ell_1 \approx -0.2387$ when $(\varepsilon, b_1) \approx (0, -0.1449)$, and $\ell_1 \approx -0.3282$ when $(\varepsilon, b_1) \approx (0, -0.2450)$, respectively. The discrepancy arises from the fact that the equation for the (slow) variable z contains terms involving the (fast) variable x that are linear or quadratic; we refer to [11] for more details.

If the system (4) is generic, then the torus bifurcation at $b_1 = b_1^{\mathrm{TR}}$ will be either supercritical or subcritical. In the supercritical (subcritical) case, the tori will be stable (unstable) near the bifurcation, and the diameter of their intersections with a cross-section will be proportional to $\sqrt{b_1 - b_1^{\mathrm{TR}}}$. We used numerical integration with the algorithm DOPRI853 [5] to test these predictions for system (4) with $s = -2.6$ and $\varepsilon = 0.1$. For this value of ε the torus bifurcation occurs at $b_1^{\mathrm{TR}} = -0.2405336$, to seven decimal places,
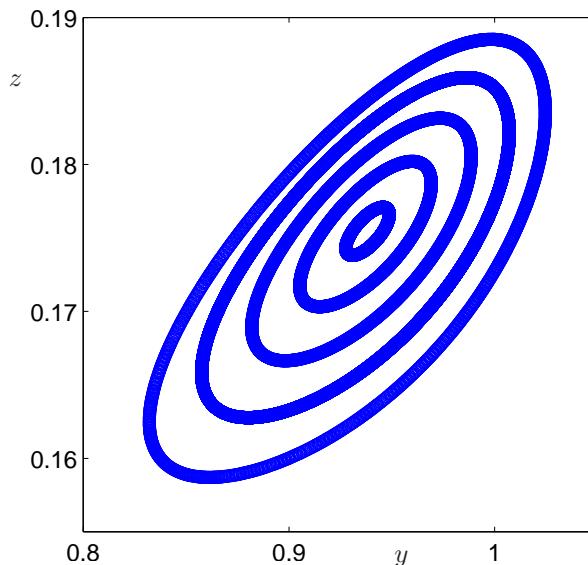
Figure 4: The torus bifurcation of system (4) with $s = -2.6$ and $\varepsilon = 0.1$ and b_1 varying is supercritical. Shown are cross-sections with the plane $x = 1.1$ of the attractor for five values of b_1, namely, $b_1 = -0.2405326, -0.2405246, -0.2405086, -0.2404846, -0.2404526$, respectively. The attractors are each obtained as the limit set of a long trajectory segment computed until transients died away; then intersections with the cross-section were computed for an additional $10,000$ time units. Each trajectory yielded over 1660 intersections with the cross-section, which are plotted in blue. The values of $b1$ increase quadratically from its value at the torus bifurcation, and the cross-sectional diameters of the tori grow linearly.

which we determined both from continuation calculations of the family Γ_{crit} and numerical integrations. Figure 4 shows the cross-section with $x = 1.1$ of five trajectories for the parameter values $b_1 = b_1^{\mathsf{TR}} + \delta_j$, where $\delta_j = (0.00j)^2$ for $j = 1, 3, 5, 7,$ and 9. For each of these values a long trajectory was computed until it appeared to be close to its limit set; the final points in these trajectories were selected as the initial point for the trajectories that are displayed in the figure. The figure clearly indicates that the torus bifurcation is supercritical with the predicted growth in the cross-sectional diameter of the tori and that any phase locking on these tori is weak.

10

3   Hopf bifurcation in a model with rotational symmetry

Our goal is to investigate whether the observations for the Hindmarsh–Rose model (4) are generic for slow-fast systems with a Hopf bifurcation in the fast variables. Therefore, we introduce the following simpler model (in cylindrical coordinates) that couples the low-order terms of the normal form (3) with a slow variable z:

$$\begin{cases} \dot{r} & = & r\,(\lambda + a\,r^2 + z), \\ \dot{\vartheta} & = & \omega, \\ \dot{z} & = & \varepsilon\,(b + c\,r^2 + d\,z). \end{cases} \qquad (6)$$

System (6) consists of low-order terms in the Taylor expansion of a general slow-fast system that is symmetric with respect to rotations around the z-axis. Note that the equation for the slow variable z is an affine function that also maintains the symmetry of rotation around the z-axis. The coupling of the slow and fast variables in (6) is similar to that of the Hindmarsh–Rose model (4); we could think of λ and a in (6) as playing the role of a and s in (4), respectively, and the parameters b, c and d in (6) are effectively b_1, a_1 and k in (4), respectively. Unfortunately, the Hindmarsh–Rose model (4) does not have rotational symmetry, — note the replacement of the linear term $s\,a_1\,x$ in (4) with the quadratic term $c\,r^2$ in (6) — but one would expect that an appropriate coordinate transformation could bring (4) in the form of (6) with additional higher-order terms that do not qualitatively alter its behavior. In fact, not all of the dynamics that we analyze for system (6) persist with the addition of higher-order terms; in particular, the stability of its invariant tori can change and we explain this further in Section 3.3. Furthermore, it is not possible to transform a system like the Hindmarsh–Rose model (4) into system (6) with rotational symmetry such that the slow-fast structure of the equations is preserved, unless the z-equation already possesses this symmetry; we explain this further in Section 3.4.

With system (6) we can reproduce the phenomena observed for the Hindmarsh–Rose model (4). Figure 5 shows bifurcation diagrams that are similar to those shown in Figures 2 and 3. Here, the bifurcation parameter is b, which plays the same role as b_1 in (4) and we fixed $\lambda = 1$ and $d = -1$. Row (a) of Figure 5 should be compared with Figure 2; the parameters $a = -\frac{1}{2}$ and $c = \frac{1}{4}$ are chosen such that the Hopf bifurcation H at $b = -1$ is supercritical and the corresponding Hopf bifurcation $\mathsf{H}_{\mathrm{crit}}$ of the layer
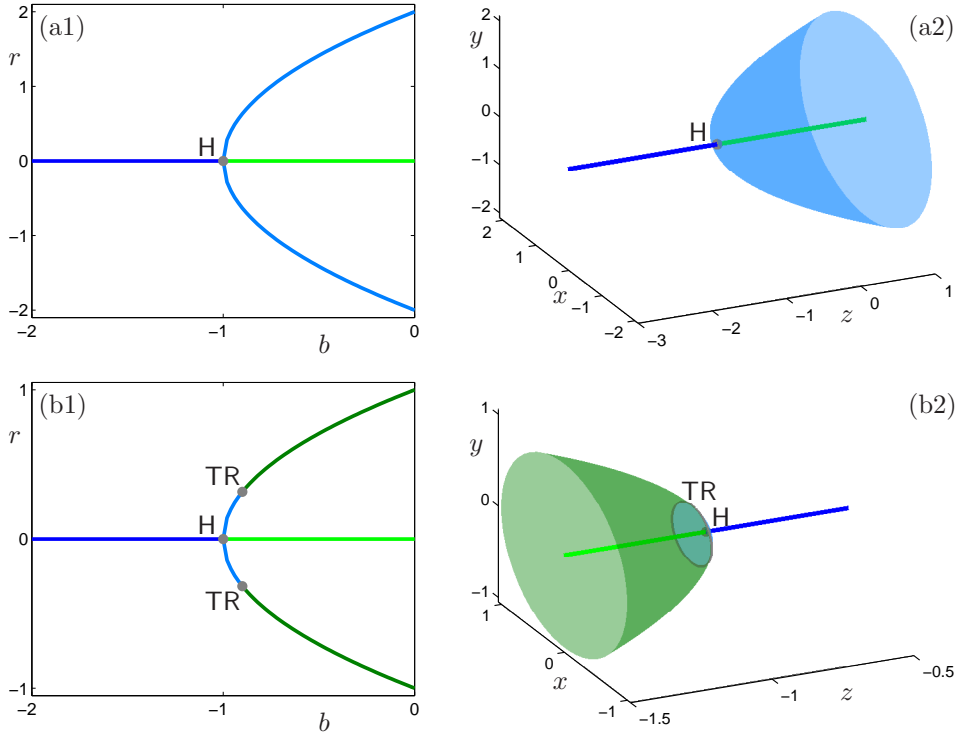
11

Figure 5: Supercritical Hopf bifurcation of system (6), where b is the bifurcation parameter. We fixed $\lambda = 1$, $d = -1$ and $\varepsilon = 0.1$; row (a) shows the case with $a = -\frac{1}{2}$ and $c = \frac{1}{4}$ and row (b) shows the case with $a = \frac{1}{2}$ and $c = -\frac{3}{2}$. In both cases the Hopf bifurcation occurs at $b = -1$ and the case in row (b) also exhibits a torus bifurcation, which occurs at $b = -0.9$. The first column shows the bifurcation diagram, where we plot r versus b; for ease of comparison with Figures 2 and Figures 3, we plot both r and $-r$ indicating the amplitudes of the periodic orbits. The second column shows the b-dependent families of equilibria and periodic orbits in (x, y, z)-space, where $x = r \cos \vartheta$, $y = r \sin \vartheta$ and z is plotted along a horizontal axis.

equations is supercritical as well. The bifurcation diagram is projected onto the (b, r)-plane in Figure 5(a1), where we plot $\pm r$ to indicate the amplitude of the family of periodic orbits, and into (x, y, z)-space in Figure 5(a2); in this latter projection we defined $x = r \cos \vartheta$ and $y = r \sin \vartheta$. Row (b) of

12

Figure 5 should be compared with Figure 3; here, the parameters are $a = \frac{1}{2}$ and $c = -\frac{3}{2}$, such that H at $b = -1$ is supercritical, but the corresponding Hopf bifurcation $\mathsf{H}_{\mathrm{crit}}$ of the layer equations is subcritical. As in Figure 3, a torus bifurcation occurs, due to the difference in criticality of the two Hopf bifurcations H and $\mathsf{H}_{\mathrm{crit}}$; only the location of the torus bifurcation actually depends on ε and we set $\varepsilon = 0.1$ in Figure 5, so that it lies at $b = -0.9$. Note that the family of periodic orbits, when projected onto (x, y, z)-space in Figure 5(b2) is oriented in the opposite direction compared to Figure 5(a2).

System (6) is amenable to a complete theoretical analysis of the phenomena observed for the Hindmarsh–Rose model (4). In the next section we consider the layer equations of (6), followed by a complete study of the Hopf bifurcation in Section 3.2 and the nature of the torus bifurcations in Section 3.3. We give details on the genericity of these phenomena in Section 3.4.

3.1 Hopf bifurcation in the layer equations

The layer equations of (6) have a line of equilibria defined by $r = 0$ that comprise the critical manifold S_{crit} of the system. The fast subsystem (r, ϑ) for a single layer, defined by fixing z, is the standard normal form for a Hopf bifurcation; see, for example, [4] where the same notation for the parameters is used. Hence, a is the Lyapunov coefficient that determines the criticality of the Hopf bifurcation, denoted $\mathsf{H}_{\mathrm{crit}}$. The effect of z is to translate $\mathsf{H}_{\mathrm{crit}}$ away from $\lambda = 0$; the Hopf bifurcation occurs at $\lambda = -z$. Fixing λ and varying z, the origin $(r = 0)$ is a dynamic Hopf bifurcation of the layer equation which occurs at $z = -\lambda$. With either interpretation, the Hopf bifurcation $\mathsf{H}_{\mathrm{crit}}$ is supercritical if $a < 0$ and subcritical if $a > 0$. For $a < 0$, a family Γ_{crit} of stable periodic orbits exists for $z > -\lambda$, whereas for $a > 0$, the family Γ_{crit} contains unstable periodic orbits that exist for $z < -\lambda$; in both cases, Γ_{crit} is defined by $r = \sqrt{|\lambda + z|/|a|}$.

It is important to realize that the examples of the Hindmarsh–Rose model (4) and system (6) have the property that the bifurcation parameters, b_1 for (4) and b for (6), appear only in the equation for the slow variable z. As a consequence, the layer equations only depend on z, but not on b_1 or b, respectively. This means that there is an obvious choice for the Hopf bifurcation $\mathsf{H}_{\mathrm{crit}}$ of the layer equations that corresponds to the Hopf bifurcation H in the full system. Since λ is the bifurcation parameter for the normal form of the Hopf bifurcation, it seems logical to choose λ as the additional bifurcation parameter also for the singularly perturbed system (6). Then both the

full system and the layer equations depend on the bifurcation parameter and we obtain a curve of Hopf bifurcations $\mathsf{H}_{\mathrm{crit}}$. Hence, the perceived accumulation of the invariant objects for the Hindmarsh–Rose model (4) as $\varepsilon \to 0$ onto the corresponding invariant objects of the layer equations is actually less straightforward. We make this distinction between bifurcation parameters explicit by considering both b and λ as candidates for the bifurcation parameter, that is, we consider the case where the layer equations depend on the bifurcation parameter as well as the case where it does not.

3.2 Hopf bifurcation in the full three-dimensional system

As soon as $\varepsilon > 0$, we must consider the full three-dimensional slow-fast system (6). The system has a circular symmetry, so we can reduce its analysis to the coordinates (r, z) where the reflection symmetry $(r, z) \to (-r, z)$ is a vestige of the original circular symmetry. Equilibria of the reduced system with $r > 0$ correspond to periodic orbits of the original system, and their stability gives the stability of the periodic orbits. The Hopf bifurcation H of system (6) occurs at the point $(r, z) = (0, -b/d)$ when $\lambda = b/d$. The point $(r, z) = (0, -b/d)$ corresponds to an actual equilibrium of the full system and we assume that this equilibrium is stable "before" the Hopf bifurcation, that is, for $\lambda < b/d$ if λ is the bifurcation parameter, or $b < 0$ if b plays this role. This means that we must have $d < 0$.

We can establish the criticality of H via a center manifold reduction. To this end, we consider the coordinate transformation $w = z + b/d + e\,r^2$ and calculate

$$
\begin{aligned}
\dot{w} &= \varepsilon(b + c\,r^2 + d\,z) + 2\,e\,r^2\,(\lambda + a\,r^2 + z) \\
&= \varepsilon\,d\,w + (\varepsilon\,c - \varepsilon\,d\,e + 2\,e\,(\lambda - b/d))\,r^2 + 2\,e\,r^2\,w + 2\,a\,e\,r^4 - 2\,e^2\,r^4.
\end{aligned}
$$

We now set $e := c/d$, which removes the quadratic term at the Hopf bifurcation when $\lambda = b/d$. This means that the cubic term of the r-equation in the new coordinates will again be given by the Lyapunov coefficient. We find

$$
\dot{r} = r\left(\lambda - \frac{b}{d} + \left(a - \frac{c}{d}\right)r^2 + w\right),
$$

with Lyapunov coefficient $a - c/d$. Hence, the criticality of the Hopf bifurcation H at $\lambda = b/d$ for the full three-dimensional slow-fast system (6) does

not depend on ε. Recall that we assume $d < 0$, so that H can have opposite criticality from that of the fast subsystem if a and c have opposite signs. In particular, when $a > 0$, so that $\mathsf{H}_{\mathrm{crit}}$ is subcritical, and c is such that $c < ad < 0$, then H is supercritical, as is the case for the Hindmarsh–Rose model (4); see also Figure 5(b).

Figures 2 and 3 give the impression that the family $\Gamma(b_1)$ of periodic orbits that emanates from the Hopf bifurcation H in the Hindmarsh–Rose model (4) accumulates onto the family Γ_{crit} of periodic orbits of the fast subsystem, regardless of a possible change in criticality for $\mathsf{H}_{\mathrm{crit}}$. We can analyze this behavior more precisely using the simplified system (6). The bifurcation H of (6) gives rise to a family of stable periodic orbits with

$$r = \sqrt{\frac{-d\,\lambda + b}{a\,d - c}} \quad \text{and} \quad z = \frac{-b - c\,r^2}{d} = \frac{c\,\lambda - a\,b}{a\,d - c},$$

that surround the origin for $\lambda > b/d$ if H is supercritical, that is, if $a - c/d < 0$, or for $\lambda < b/d$ if $a - c/d > 0$.

The family Γ_{crit} defined by the layer equations of system (6) satisfies $\lambda + a\,r^2 + z = 0$, that is, we have a λ-dependent family of periodic orbits

$$r = \sqrt{\frac{\lambda + z}{-a}}$$

that is parameterized by z. If λ is fixed and b acts as the bifurcation parameter, then Γ_{crit} is the same family for all b. The family $\Gamma(b)$ lies on this surface of curves Γ_{crit}, as illustrated in Figure 6(a) for $\lambda = 0$. If we fix b, on the other hand, then Γ_{crit} changes with λ and it is the location of the family $\Gamma(\lambda)$ on this surface that is determined by b; this situation is illustrated for $b = 0$ in Figure 6(b). Both panels in Figure 6 show Γ_{crit} as a (green) surface and $\Gamma(b)$ or $\Gamma(\lambda)$ as a thick (blue) curve for system (6) with $a = \frac{1}{2}$, $c = -\frac{3}{2}$ and $d = -1$. The value of $\varepsilon > 0$ is arbitrary, because the respective families do not depend on ε. The thick (red) curve in the (z, r)-plane where the bifurcation parameter, b or λ, is zero illustrates that the projection onto (r, z)-space, or more precisely, (r, ϑ, z)-space, is the same for both families. Indeed, from

$$z = \frac{c\,\lambda - a\,b}{a\,d - c} \Leftrightarrow \frac{b}{a\,d - c} = \frac{c\,\lambda}{a\,(a\,d - c)} - \frac{z}{a},$$

we find

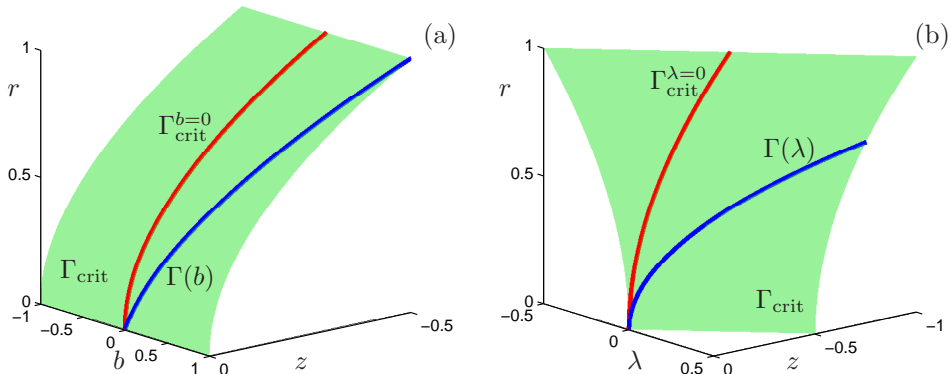$$r = \sqrt{\frac{-d\,\lambda + b}{a\,d - c}} = \sqrt{\frac{-\lambda - z}{a}}.$$

15

Figure 6: System (6) with $a = \frac{1}{2}$, $c = -\frac{3}{2}$, $d = -1$ and $\varepsilon > 0$ arbitrary, has a one-parameter family $\Gamma(b)$ of periodic orbits, shown for $\lambda = 0$ in panel (a), and a one-parameter family $\Gamma(\lambda)$ of periodic orbits, shown for $b = 0$ in panel (b), that lie on the two-parameter surface Γ_{crit} parameterized by the slow variable z and the bifurcation parameter. In panel (a), the surface Γ_{crit} does not depend on b, but the value of λ determines its location in (b, z, r)-space. In panel (b), the surface Γ_{crit} depends on both λ and z, and the value of b determines the location of $\Gamma(\lambda)$ on this surface.

Hence, despite the fact that the family of periodic orbits emanating from H under variation of a parameter is not the same as the family Γ_{crit}, which is strictly speaking a higher-dimensional manifold, the respective projections onto the phase space of the full system (6) are identical.

3.3 The torus bifurcation

We can show that a difference in criticality between the Hopf bifurcations H of the full system and H_{crit} of the fast subsystem must give rise to a torus bifurcation TR as illustrated in Figure 3. To simplify the algebra, we translate the Hopf bifurcation point $(r, z, \lambda) \mapsto (r, z + b/d, \lambda - b/d)$ of system (6) to the origin and rescale time by the factor $-d$. This leads to the reduced system

$$\begin{cases} \dot{r} &= r\left(-\frac{\lambda}{d} + \frac{b}{d^2} - \frac{a}{d}r^2 + z\right), \\ \dot{z} &= \varepsilon\left(\frac{c}{d^2}r^2 - z\right), \end{cases}$$

16

which has the same form as system (6) with $b = 0$, $d = -1$, and λ, a and c replaced by $-\lambda/d + b/d^2$, $-a/d$ and c/d^2, respectively. Hence, we revert to system (6) and assume $b = 0$ and $d = -1$.

Let us now consider the particular case where system (6) undergoes a supercritical Hopf bifurcation H, which occurs at $\lambda = 0$, but $a > 0$ so that $\mathsf{H}_{\mathrm{crit}}$ is subcritical, independent of λ. This means that $c < -a < 0$ such that $a + c < 0$. The stability of the family of periodic orbits that bifurcates from H is determined by the Jacobian matrix of the reduced system at such points, which is given by

$$\mathrm{Jac}(r,\, z) = \begin{pmatrix} \lambda + 3\, a\, r^2 + z & r \\ 2\, \varepsilon\, c\, r & \varepsilon\, d \end{pmatrix} \Bigg|_{(r,\, z) = \left(\sqrt{\frac{-\lambda}{a+c}},\, \frac{-\lambda\, c}{a+c} \right)} = \begin{pmatrix} \frac{-2\, a\, \lambda}{a+c} & \sqrt{\frac{-\lambda}{a+c}} \\ 2\, \varepsilon\, c\, \sqrt{\frac{-\lambda}{a+c}} & -\varepsilon \end{pmatrix}.$$

Note that the determinant of this matrix is $2\, \varepsilon\, \lambda$, which is positive for $\lambda > 0$. Its trace is negative for sufficiently small $\lambda > 0$, so the periodic orbits are stable, but the family becomes unstable in a torus bifurcation TR as soon as this trace changes sign, that is, when

$$\frac{-2\, a\, \lambda}{a+c} - \varepsilon = 0 \Leftrightarrow \lambda = \frac{-(a+c)}{2\, a} \varepsilon > 0.$$

We observe that the torus bifurcation TR occurs for $\lambda = O(\varepsilon)$, approaching the Hopf bifurcation H as $\varepsilon \to 0$. Hence, when the parameters are such that the criticality of $\mathsf{H}_{\mathrm{crit}}$ and H are opposite, a torus bifurcation TR at distance $O(\varepsilon)$ away from H changes the stability of the family of periodic orbits 'back' to what is predicted from $\mathsf{H}_{\mathrm{crit}}$ in the singular limit.

Unfortunately, system (6) does not provide further insight into the behavior near a singularly perturbed Hopf bifurcation. The torus bifurcation of system (6) is totally degenerate: at the torus bifurcation, the system is integrable and a (vertical) one-parameter family of invariant tori exists only for this particular parameter value. We have the following result:

Theorem 3.1. *The torus bifurcation of system (6) at $\lambda = \frac{-(a+c)}{2\, a} \varepsilon$, $a > 0$, $b = 0$, $c < -a < 0$ and $d = -1$ is totally degenerate: there is a one-parameter family of tori that surrounds the neutrally stable periodic orbit of this system. This family is bounded by the parabolic cylinder $z + a\, r^2 = 0$ and the line $r = 0$.*

To demonstrate this fact, we fix the value of λ at its torus bifurcation value, introduce new coordinates for system (6) by setting $r = \rho^\beta$ with $\beta =$
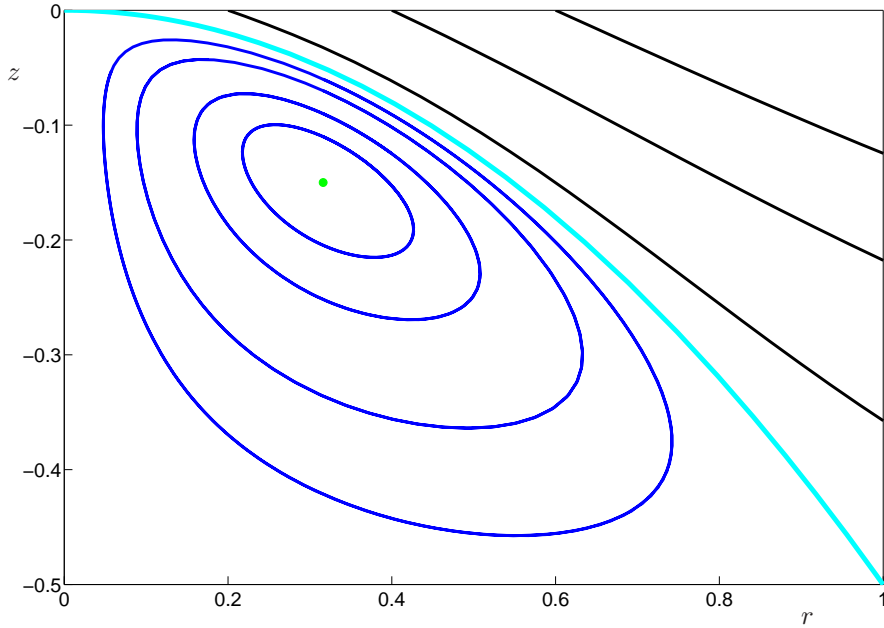
Figure 7: Phase portrait of system (6) projected onto the (r, z)-plane. The parameters are $\lambda = 0.1$, $a = \frac{1}{2}$, $b = 0$, $c = -\frac{3}{2}$, $d = -1$ and $\varepsilon = 0.1$ where a torus bifurcation takes place. The figure illustrates that there is a family of invariant tori (blue closed curves) bounded by the surface $z = -\frac{1}{2}r^2$ (thick cyan curve) and the z-axis.

$\lambda/\varepsilon = -\frac{a+c}{2a}$ and rescale the system by a factor $\exp(\gamma z)$ with $\gamma = 1/\lambda = -\frac{2a}{\varepsilon(a+c)}$ to produce the system

$$\begin{cases} \dot{\rho} &= \rho \exp(\gamma z) \left(-\varepsilon + \frac{2a^2}{a+c} \rho^{-\frac{a+c}{a}} + \frac{2a}{a+c} z\right), \\ \dot{z} &= \varepsilon \exp(\gamma z) \left(z - c \rho^{-\frac{a+c}{a}}\right), \end{cases} \qquad (7)$$

where we have suppressed the equation for ϑ. System (7) is divergence free and has first integral

$$\begin{aligned} h(\rho, z) &= \varepsilon \rho \exp(\gamma z) \left(a \rho^{2\beta} + z\right) \\ &= \varepsilon \rho \exp\left(-\frac{2 a z}{\varepsilon (a + c)}\right) \left(a \rho^{-\frac{a+c}{a}} + z\right). \end{aligned}$$

Figure 7 displays a phase portrait of the integrable system. We fixed $a = \frac{1}{2}$,

18

$b = 0$, $c = -\frac{3}{2}$, $d = -1$ and $\varepsilon = 0.1$ in system (6), so that the torus bifurcation occurs at $\lambda = \varepsilon = 0.1$. Both the parabolic cylinder $z + a\,r^2 = 0$ (thick cyan curve) and the line $r = 0$ are zero-level sets of $h(\rho, z)$, since $\rho = r^{1/\beta}$. We verified numerically that the level sets form bounded closed curves (colored blue) only for (r, z) inside this region, where $h(\rho, z) < 0$.

3.4   Genericity of the bifurcation phenomena

System (6) is the paradigm model for the phenomena observed for the Hindmarsh–Rose model (4) and it plays an essential role in the proof of Theorem 1.1 stated in the Introduction. Indeed, we believe that system (6) correctly identifies the criteria for the existence of a torus bifurcation, even though its torus bifurcations are degenerate.

There is an ε-dependent scaling that eliminates ε from the dynamics of system (6): namely, set $r = \varepsilon^{1/2}R$, $z = \varepsilon Z$, $\lambda = \varepsilon\Lambda$, $b = \varepsilon B$ and $T = \varepsilon t$ in system (6) to yield

$$\begin{cases} R' &= R\,(\Lambda + a\,R^2 + Z), \\ Z' &= B + c\,R^2 + d\,Z. \end{cases}$$

Since this last system is independent of ε, the scaling shows exactly how the dynamics of the original system (6) depend upon ε. Moreover, higher-order terms in a Taylor expansion of system (6) will tend to zero with this scaling, suggesting that the dynamics displayed by (6) are universal — apart from the degeneracy of the family of tori. In particular, when the first Lyapunov coefficients $\ell_1(0)$ and $\ell_1(\text{layer})$ have opposite signs, there will be a torus bifurcation. Furthermore, the difference between the parameters at which the torus and Hopf bifurcations occur has magnitude $\beta\varepsilon$ with β determined by the Taylor coefficients of the system.

In dynamical systems with a single time scale, normal forms have been central to the analysis of bifurcations. The theory of normal forms seeks model systems that have the following two properties:

- Every family undergoing bifurcation can be transformed to a normal form, up to higher-order terms of a Taylor expansion.

- The normal form family is structurally stable — perturbations of the family produce topologically equivalent families.

The model system (6) that is the focus of our analysis satisfies neither of these properties. It clearly does not have the second property because of the neutral stability of its invariant tori, but this can be remedied by the addition of appropriate higher-order terms in either the fast or slow equations. Normal forms for codimension-two zero-Hopf bifurcations [4] are a closely related example in which this phenomenon has been analyzed.

With regard to the first property, normal forms for slow-fast systems should respect the slow-fast structure. This means that coordinate changes $(u, v) = h(x, y)$ used to transform system (1) to a normal form should have the property that v depends only on the slow variable y. If one restricts coordinate changes to ones that have this property, then perturbations of the model system (6) in which $\dot{z}$ fails to have rotational symmetry cannot be transformed to ones that do. On the other hand, symmetric normal forms can be achieved by coordinate changes that alter the slow-fast structure by $O(\varepsilon)$. Transformations in which v is a function of $(\varepsilon x, y)$ still yield a slow-fast system and are sufficiently general to complete the reduction to normal form. The transformed fast equations are ε-dependent, but a tedious calculation shows that the change in its first Lyapunov coefficient is $O(\varepsilon)$.

Here are a few details of these normal form calculations. Consider a system of the form

$$
\begin{array}{rcl}
\dot{x} & = & -\omega\, y + x\, (\lambda + a\, (x^2 + y^2) + z), \\
\dot{y} & = & \omega\, x + y\, (\lambda + a\, (x^2 + y^2) + z), \\
\dot{z} & = & \varepsilon\, (b + s\, x + c\, (x^2 + y^2) + d\, z),
\end{array}
$$

that adds an asymmetric linear term to the equation for $\dot{z}$ in system (6). As above, we reduce to the case $b = 0$ that places the equilibrium at the origin and set $\lambda = 0$ where the Hopf bifurcation occurs. We want to compute the contribution of the term $s\, x$ in the equation for $\dot{z}$ to the first Lyapunov coefficient. The Jacobian is no longer in Jordan form: its right eigenvectors are $(\varepsilon\, d \pm \omega\, i,\ \omega \mp \varepsilon\, d\, i,\ \varepsilon\, s)^T$ and $(0,\, 0,\, 1)^T$. To order ε, a linear change of coordinates to (u, v, w) that restores Jordan form produces terms proportional to $\varepsilon\, s\, u\, w$ and $\varepsilon\, s\, v\, w$ in the equation for $\dot{w}$. When performing a center manifold reduction, these terms do not affect the first Lyapunov coefficient. There are also new quadratic terms proportional to s in the equations for $\dot{u}$ and $\dot{v}$, but these are $O(\varepsilon)$ and do not produce an $O(1)$ change in the first Lyapunov coefficient. In contrast, the quadratic terms $\varepsilon\, c\, (x^2 + y^2)$ of $\dot{z}$ do produce $O(1)$ changes in the first Lyapunov coefficient as we saw in the argument above. These calculations confirm that the system (6) represents a normal form for

Hopf bifurcation with fast eigenvalues of a slow-fast system, provided that coordinate transformations are allowed that alter the slow-fast structure by $O(\varepsilon)$. We conclude that systems with Hopf bifurcations in their fast variables also have nearby torus bifurcations when the first Lyapunov coefficients $\ell_1(0)$ and $\ell_1(\text{layer})$ have opposite signs. While the original slow-fast structure may be lost, the time-scale separation of oscillation frequencies on the invariant tori remains intact.

4   Conclusions

We have analyzed Hopf bifurcations that occur in slow-fast systems where the eigenvectors of the purely imaginary eigenvalues are oriented in fast directions. As a motivating example, we used a model of Hindmarsh–Rose type that is used as a paradigm model for bursting patterns in neurons [14, 20]. We introduced a simpler model in cylindrical polar coordinates for which all computations can be done explicitly. The Hopf bifurcation H has a singular limit that corresponds to a Hopf bifurcation H_{crit} in the layer equations. Similarly, we found that the first Lyapunov coefficient of H has a singular limit, but this limit does not agree with the first Lyapunov coefficient of the corresponding H_{crit}; in fact, they can even have opposite signs. When the signs of these Lyapunov coefficients differ, oscillations that couple slow and fast variables appear near periodic orbits of small amplitude and give rise to torus bifurcations. The stability of the invariant tori emerging from this bifurcation depends upon higher-order terms in a Taylor series expansion, analogous to the invariant tori appearing in the unfolding of a codimension-two fold-Hopf bifurcation of an equilibrium with a zero eigenvalue and a pair of purely imaginary eigenvalues [4]. In examples, parameter ranges with attracting invariant tori are likely to be small, but not "exponentially" small, if the Taylor expansions contain generic higher-order terms.

The role of parameters in the singular limit of a slow-fast system remains a confusing aspect of our investigations. The slow variables of a system become parameters of the layer equations whose equilibrium points constitute the entire critical manifold of the system. Equilibrium points of the full system typically have a well-defined limit determined by the slow equations, but the distinction between different points of the critical manifold is largely lost in the layer equations themselves. While varying a single parameter μ of the full system, an isolated Hopf bifurcation H is replaced in the family of layer

equations by a codimension-one manifold of Hopf bifurcations H_{crit}, that is, the family H_{crit} has the same dimension as the critical manifold. Thus it can be awkward to identify "the" Hopf bifurcation H_{crit} of the layer equation, and there are different cases that depend upon how μ enters the system.

If μ appears in each fast subsystem and the appropriate eigenvalues cross the imaginary axis transversally as μ varies, then each fast subsystem in a region of slow-variable parameters will have a Hopf bifurcation. This is the case when $\mu = \lambda$ in the system (6). By selecting the slow variables at the limit of H as $\varepsilon \to 0$, we identify a fast subsystem and a Hopf bifurcation point on the family H_{crit} that is naturally compared with the Hopf bifurcation H of the full system.

On the other hand, we have highlighted circumstances where μ appears only in the slow equations, for example when $\mu = b$ in the system (6). In these circumstances, the layer equations do not depend on μ at all. In this situation, the typical behavior will be that there is a codimension-one set of slow variables that have equilibrium points with purely imaginary eigenvalues. Varying a slow variable transverse to this submanifold is necessary for the real parts of the eigenvalues to change in the layer equations. The whole manifold of Hopf bifurcations H_{crit} still has the same dimension as the critical manifold, but it is fibered by lines parallel to the μ-axis. While we can still identify a Hopf bifurcation point on the family H_{crit} that corresponds to the Hopf bifurcation point H in the full system, varying μ in the fast subsystem through this point does not produce a Hopf bifurcation: one of the slow variables must be used as a parameter to obtain the bifurcation. Setting the value of this parameter at the bifurcation, we can find the value of μ that gives the limit of the desired equilibria of the full system as $\varepsilon \to 0$. These issues of parameter dependence are one more way in which the singular limit of a slow-fast system is truly singular. Despite these differences, we have found that the families of periodic orbits emanating from the Hopf bifurcation of the full system approach those of a suitably chosen one parameter family undergoing Hopf bifurcation in the layer system.

Acknowledgements

References

[1] B. Braaksma, *Singular Hopf bifurcation in systems with fast and slow variables*, J. Nonlin. Sci. **8**(5) (1998), 457–490.

[2] M. Desroches, B. Krauskopf, and H. M. Osinga, *The geometry of slow manifolds near a folded node*, SIAM J. Appl. Dyn. Syst., 7(4):1131–1162, 2008.

[3] A. Dhooge, W. Govaerts and Yu. A. Kuznetsov, *MATCONT: A Matlab package for numerical bifurcation analysis of ODEs*, ACM Trans. Math. Software **29** (2003), 141–164.

[4] J. Guckenheimer and P. Holmes. "Nonlinear Oscillations, Dynamical Systems and Bifurcations of Vector Fields," 2nd edition, Springer-Verlag, New York/Berlin, 1986.

[5] E. Hairer, S. P. Nrsett and G. Wanner. "Solving ordinary differential equations. I. Nonstiff problems," 2nd edition, Springer-Verlag, Berlin, 1993.

[6] J. Hindmarsh and M. Rose, *A model of neuronal bursting using three coupled first order differential equations*, Proc. R. Soc. London **B221** (1984), 87–102.

[7] A. L. Hodgkin and A. F. Huxley, *A quantitative description of membrane current and its application to conduction and excitation in nerve*, J. Physiol. (London) **117** (1952), 205–249.

[8] F. C. Hoppensteadt and E. M. Izhikevich, "Weakly Connected Neural Networks," Springer-Verlag, New York/Berlin, 1997.

[9] E. M. Izhikevich, "Dynamical Systems in Neuroscience: the Geometry of Excitability and Bursting," Computational Neuroscience, MIT Press, Cambridge, Mass., 2007.

[10] J. Keener and J. Sneyd, "Mathematical Physiology," 2nd edition, Springer-Verlag, New York 2008.

[11] W. Zhang, V. Kirk, J. Sneyd, and M. Wechselberger, *Physiological model reduction techniques and computing the criticality of Hopf bifurcations in systems with multiple time scales*, preprint, 2011.

[12] Yu. A. Kuznetsov, "Elements of Applied Bifurcation Theory," 3rd edition, Springer-Verlag, New York/Berlin, 2004.

[13] H. M. Osinga, A. Sherman, and K. T. Tsaneva-Atanasova, *Cross-currents between biology and mathematics on models of bursting*, Discr. Cont. Dyn. Sys. Ser. A **??** (2011), ??–??.

[14] H. M. Osinga and K. T. Tsaneva-Atanasova, *Dynamics of plateau bursting depending on the location of its equilibrium*, J. Neuroendocrinology **22**(12) (2010), 1301–1314.

[15] B. van der Pol, *A theory of the amplitude of free and forced triode vibrations*, Radio Review **1** (1920), 701–710.

[16] B. van der Pol, *On relaxation oscillations*, Philosophical Magazine **7** (1926), 978–992.

[17] J. Rinzel, *A formal classification of bursting mechanisms in excitable systems*, in "Proc. Intl. Cong. Math. (ed. A. M. Gleason), American Mathematical Society (1987) 1578–1593).

[18] H. G. Rotstein, T. Oppermann, J. A. White, and N. Kopell, *The dynamic structure underlying subthreshold oscillatory activity and the onset of spikes in a model of medial entorhinal cortex stellate cells*, J. Comput. Neurosci. **21** (2006), 271–292.

[19] A. Shilnikov and M. Kolomiets, *Methods of the qualitative theory for the Hindmarsh–Rose model: A case study. A tutorial*, Int. J. Bifurcat. Chaos **18**(8) (2008), 2141–2168.

[20] K. T. Tsaneva-Atanasova, H. M. Osinga, T. Rieß, and A. Sherman, *Full system bifurcation analysis of endocrine bursting models*, J. Theoretical Biology **264**(4) (2010), 1133–1146.